Oxidized Divinyl Oligoacene-Bridged Diruthenium Complexes: Bridge Localized Radical Characters and Reduced Aromaticity in Bridge Cores

Ya-Ping Ou,[a, b, c] Jing Zhang,[b] Yuxuan Hu,[b] Jun Yin,[b] Chunyan Chi,[c] Sheng Hua Liu*[b]

[a]*Key Laboratory of Functional Metal-Organic Compounds of Hunan Province, Key Laboratory of Functional Organometallic Materials of Hunan Province College, College of Chemistry and Material Science, Hengyang Normal University, Hengyang, Hunan 421008, P.R. China*
[b]*Key Laboratory of Pesticide and Chemical Biology, Ministry of Education, College of Chemistry, Central China Normal University, Wuhan 430079, P.R. China*
[c]*Department of Chemistry, National University of Singapore, 3 Science Drive 3, 117543, Singapore*

Supporting Information

TABLE OF CONTENTS

1. Experimental section

1.1 General Materials and Physical Measurements

All manipulations were carried out at room temperature under a nitrogen atmosphere using standard Schlenk techniques, unless otherwise stated. Solvents were predried, distilled, and degassed prior to use, except those for spectroscopic measurements, which were of spectroscopic grade. The reagent $Pd(PPh_3)_4$, (trimethylsilyl)acetylene (TMSA) and starting material 1,4-dibromonaphthalene (**2a**) were commercially available. Other starting materials $RuHCl(CO)(PPh_3)_3$[1], 1,4-dibromoanthracene (**3a**)[2], tetracene-5,12-dione (**5a**)[3] and target complexes **1**[4] and **4**[5] were prepared according to the procedures described in literature methods.

^1H, ^{13}C, and ^{31}P NMR spectra were collected on a Varian Mercury Plus 400 spectrometer (400 MHz). ^1H and ^{13}C NMR chemical shifts are relative to TMS, and ^{31}P NMR chemical shifts are relative to 85% H_3PO_4. Elemental analyses (C, H, N) were performed with a Vario ElIII Chnso instrument. IR and UV–Vis–NIR spectroelectrochemistry experiments were recorded using Nicolet Avatar spectrometer or a Shimadzu UV-3600 UV–Vis–NIR spectrophotometer respectively by spectroelectrochemical (SEC) liquid sample cells GS20900 series with a path length of 200 μm.[6] Solid IR spectra was recorded using a Nicolet Avatar spectrometer from Nujol mull suspended between KBr discs. The electrochemical measurements were performed on a CHI 660C potentiostat (CHI USA). A three-electrode one-compartment cell was used to contain the solution of complexes and supporting electrolyte in dry CH_2Cl_2. Deaeration of the solution was achieved by argon bubbling through the solution for about 10 min before measurement. The ligand and electrolyte ($^nBu_4NPF_6$) concentrations were typically 0.001 and 0.1 mol dm^{-3}, respectively. A 500 μm diameter platinum-disk working electrode, a platinum-wire counter electrode, and an Ag/Ag^+ reference electrode were used. The Ag/Ag^+ reference electrode contained an internal. The EPR spectra of singly-oxidized species generated by adding 1.0 eq chemical oxidant (ferrocenium hexafluorophosphate) into the solution of charge neutral molecules was recorded on a Bruker BioSpin GmbH, using a microwave frequency of about 9.84 GHz, 100 kHz modulation frequency, 1 G modulation amplitude, and *ca* 20 mW power of the microwave.

1.2 Synthetic Procedures and Characterization Data

Synthesis of Bis((trimethylsilyl)ethynyl)oligoacene

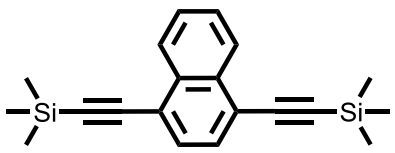

2b

1,4-Bis(trimethylsilylethynyl)naphthalene (**2b**):

To a stirred solution of 1,4-dibromonaphthalene **2a** (1.0 g, 3.5 mmol), CuI (67 mg, 0.35 mmol), and $Pd(PPh_3)_4$ (404 mg, 0.35 mmol) in triethylamine (30 mL) and THF (30 mL) under an argon atmosphere was added (trimethylsilyl)acetylene (857 mg, 8.74 mmol), and the mixture at 60 ℃ was refluxed for 24 h. The cold solution was filtered through a bed of celite. The filtrate was evaporated under reduced pressure and purified by silica gel column chromatography (petroleum ether) to give a white solid (1.05 g, 94%). ^{1}H NMR (400 MHz, $CDCl_3$): δ (ppm) 0.34 (s, 18H, $SiCH_3$), 7.60 (t, *J* = 3.2, Hz, 2H), 7.62 (d, *J* = 1.2 Hz, 2H), 8.33 (dd, *J* = 1.2 Hz, 2H).

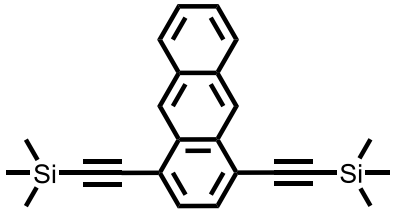

3b

1,4-Bis(trimethylsilylethynyl)anthracene (**3b**):

The procedure of **3b** was similar to that for **2b**. 1,4-dibromoanthracene **3c** (200 mg, 0.60 mmol), CuI (11 mg, 0.06 mmol), $Pd(PPh_3)_4$ (69 mg, 0.06 mmol), triethylamine (12 mL) and THF (12 mL), (trimethylsilyl)acetylene (143 mg, 1.46 mmol). Yield: 190 mg (86%) of a green solid. ^{1}H NMR (400 MHz, $CDCl_3$): δ (ppm) 0.42 (s, 18H, $SiCH_3$), 7.54 (dd, *J* = 2.8 Hz, 2H), 7.66 (d, *J* = 3.2 Hz, 2H). 8.09 (dd, *J* = 2.8 Hz, 2H), 8.91 (s, 2H). ^{13}C NMR (100 MHz, $CDCl_3$): δ (ppm) 0.09 (Si-CH_3), 101.84, 103.11, 121.68, 125.69, 126.17, 128.48, 129.69, 130.48, 132.15.

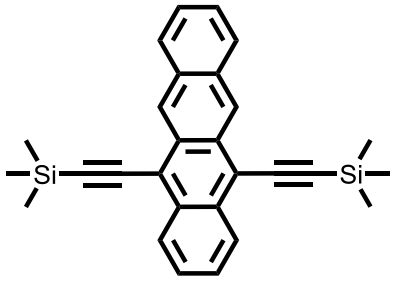

5b

5,12-Bis(trimethylsilylethynyl)tetracene (**5b**):

Under N_2 protection, to a 100 mL three-necked bottle adding successively THF (20 mL), 2 M ^{i}PrMgCl in THF (9.5 mL, 19.5 mmol), and trimethylsilylacetylene (1.95 g, 19.5 mmol) via syringe, the mixture was stirred 30 min at 60 ℃, after which was cooled to rt. **5a** (418 mg, 1.62 mmol) was directly added to reaction system. This reaction mixture was continuously stirred about 45 min at 60 ℃ until started material fully dissolved. After the reaction system is cooled down, stannous chloride ($SnCl_2$) aqueous solution is added dropwise until no bubbles are generated. Following addition of $SnCl_2$ the reaction was again heated at 60 ℃ for 15 min. The reaction was cooled to rt, the filtrate was obtained by filtered and washed by CH_2Cl_2. The filtrate was evaporated under reduced pressure and purified by silica gel column chromatography (CH_2Cl_2:PE (v/v) = 1/5) to give a red solid (400 mg, 59%). ^{1}H NMR

(400 MHz, $CDCl_3$): δ (ppm) 0.48 (Si-CH_3), 7.47 (t, *J* = 6.4 Hz, 2H), 7.54 (dd, *J* = 2.8 Hz, 2H), 8.07 (d, *J* = 9.6 Hz, 2H), 8.56 (dd, *J* = 3.2 Hz, 2H), 9.18 (s, 2H).

Synthesis of Diethynyloligoacene

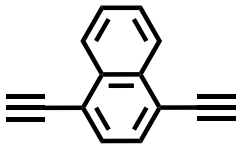

2c

1,4-Diethynylnaphthalene (**2c**):

1,4-Bis(trimethylsilylethynyl)naphthalene (**2b**) (500 mg, 0.56 mmol) was dissolved in a mixture of THF and methanol (50 mL, 1/1, v/v). Potassium hydroxide (210 mg, 3.74 mmol) was added, and the reaction mixture was stirred at room temperature for 2 h. The reaction mixture was diluted with dichloromethane and washed with brine. The organic layer was dried over Na_2SO_4, and the solvent was removed in vacuo. The crude product was purified by chromatography (petroleum ethe). Yield: 264 mg (96%) of a orange red solid. ^{1}H NMR (400 MHz, $CDCl_3$): δ (ppm) 3.40 (s, 2H, C≡CH), 7.48 (dd, *J* = 1.2 Hz, 2H), 7.53 (s, 2H). 8.35 (dd, *J* = 1.2 Hz, 2H).

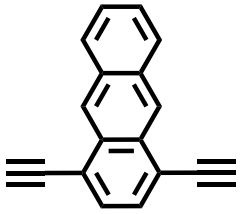

3c

1,4-Diethynylanthracene (**3c**):

The procedure of **3c** was similar to that for **2c**: **3b** (300 mg, 0.80 mmol), potassium hydroxide (109 mg, 1.94 mmol), THF (20 mL), methanol (20 mL). The crude product was purified by chromatography (petroleum ether). Yield: 160 mg (87%) of a yellow solid. ^{1}H NMR (400 MHz, $CDCl_3$): δ (ppm) 3.65 (s, 2H, C≡CH), 7.50 (dd, *J* = 3.2 Hz, 2H), 7.65 (s, 2H). 8.04 (dd, *J* = 3.6 Hz, 2H), 8.90 (s, 2H). ^{13}C NMR (100 MHz, $CDCl_3$): δ (ppm) 81.69 (C≡CH), 83.98 (C≡CH), 121.09, 125.52, 126.33, 128.36, 129.98, 130.43, 132.27.

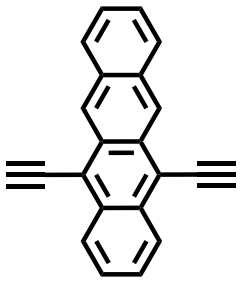

5c

5,12-Diethynyltetracene (**5c**):

The procedure of **5c** was similar to that for **2c**, just replace KOH with *n*-Bu_4NF:

5b (150 mg, 0.36 mmol), $^{n}Bu_4NF$ (454 mg, 1.44 mmol), THF (20 mL), methanol (2-3 mL). The crude product is not further purified due to its instability and poor solubility, and is directly put into next step reaction.

General Synthesis of Binuclear Ruthenium Vinyl Complexes

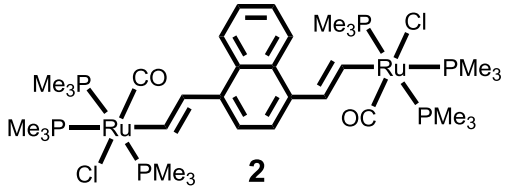

2

Preparation of **2**:

To suspension of $RuHCl(CO)(PPh_3)_3$ (541 mg, 0.57 mmol) in CH_2Cl_2 (20 mL) was slowly added a solution of diethynylnaphthalene **2c** (0.05 g, 0.28 mmol) in CH_2Cl_2 (5 mL). The reaction mixture was stirred for 30 min to give a red solution. Then a 1M THF solution of PMe_3 (2.84 mL, 2.84 mmol) was added to the red solution. The mixture was stirred for another 20 h. The solution was reduced to *ca*. 2 mL under vacuum. Addition of hexane (30 mL) to the residue produced a white solid, which was collected by filtration, washed with hexane, and dried under vacuum. Yield: 185 mg, 68%. ^{1}H NMR (400 MHz, $CDCl_3$): δ (ppm) 1.43 (t, *J*(PH) = 3.6 Hz, 36H, PMe_3), 1.51 (d, *J*(PH) = 3.6 Hz, 18H, PMe_3), 7.34-7.40 (m, 2H, Nath-CH=), 7.42 (dd, *J*(HH) = 3.6 Hz, 2H, H-5, H-8), 7.62 (s, 2H, H-2, H-3), 8.11-8.17 (m, 2H, Ru-CH=), 8.36 (dd, *J*(HH) = 3.6 Hz, 2H, H-6, H-7). ^{13}C NMR (100 MHz, $CDCl_3$): δ (ppm) 16.72 (t, *J* = 15.3 Hz, PMe_3), 20.14 (d, *J* = 20.2 Hz, PMe_3), 121.99, 123.99, 124.21, 130.09, 131.21, 135.34 (Nath-CH=), 167.02 (Ru-CH=), 202.64 (CO). ^{31}P NMR (160 MHz, $CDCl_3$): δ (ppm) -19.88 (t, *J* = 22.56 Hz, PMe_3), -7.99 (d, *J* = 22.56 Hz, PMe_3). IR (KBr/cm^{-1}): ν(CO) 1914 (s); ν(C=C) 1556 (m). Anal. Calcd for $C_{34}H_{66}Cl_2O_2P_6Ru_2$: C, 42.28; H, 6.89. Found: C, 42.40; H, 6.65.

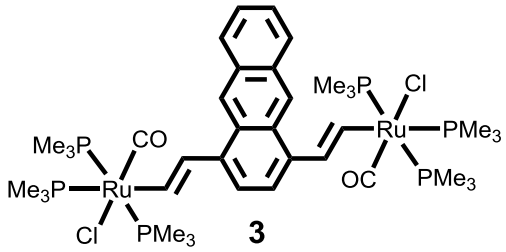

3

Preparation of **3**:

The procedure of **3** was similar to that for **2**. $RuHCl(CO)(PPh_3)_3$ (419 mg, 0.44 mmol) is dissolved in CH_2Cl_2 (20 mL), **3c** (50 mg, 0.22 mmol) is dissolved in CH_2Cl_2 (5 mL), PMe_3 (1 M THF solution) (2.20 mL, 2.20 mmol). A yellow solid was obtained. Yield: 163 mg, 72%. ^{1}H NMR (400 MHz, $CDCl_3$): δ (ppm) 1.46 (ppm) (t, *J*(PH) = 3.0 Hz, 36H, PMe_3), 1.50 (d, *J*(PH) = 6.6 Hz, 18H, PMe_3), 7.39 (t, *J*(HH) = 3.6 Hz, 2H, H-6, H-7), 7.49-7.54 (m, 2H, ant-CH=), 7.60 (s, 2H, H-2, H-3), 7.99 (t, *J*(HH) = 3.6 Hz, 2H, H-5, H-8), 8.17-8.24 (m, 2H, Ru-CH=), 8.89 (s, 2H, H-9, H-10). ^{13}C NMR (100 MHz, $CDCl_3$): δ (ppm) 16.74 (ppm) (t, *J* = 13.8 Hz, PMe_3), 20.12 (d, *J* = 20.7 Hz, PMe_3), 121.31, 122.36, 124.40, 128.37, 129.74, 130.55, 131.47, 135.47 (ant-CH=), 167.50 (Ru-CH=), 202.60 (CO). ^{31}P NMR (160 MHz, $CDCl_3$): δ (ppm)

-19.91 (ppm) (t, J = 22.56 Hz, PMe_3), -7.87 (d, J = 22.56 Hz, PMe_3). IR (KBr/cm^{-1}): ν(CO) 1914 (s); ν(C=C) 1556 (m). Anal. Calcd for $C_{38}H_{68}Cl_2O_2P_6Ru_2$: C, 44.93; H, 6.75. Found: C, 45.09; H, 6.61.

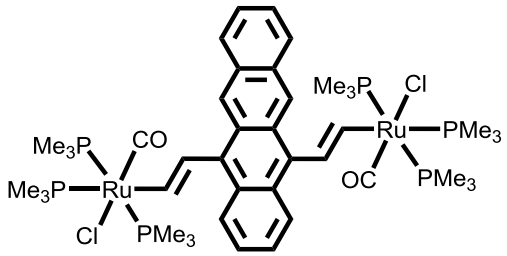

5

Preparation of **5**:

The procedure of **5** was similar to that for **2**. $RuHCl(CO)(PPh_3)_3$ (414 mg, 0.43 mmol) is dissolved in CH_2Cl_2 (20 mL), **5c** (60 mg, 0.22 mmol) is dissolved in CH_2Cl_2 (5 mL), PMe_3 (1 M THF solution) (2.17 mL, 2.17 mmol). A purple red solid was obtained. Yield: 70 mg, 30%. In addition, mono-inserted product **5d** was obtained by collecting filtrate and characterized by X-ray single diffraction. ^{1}H NMR (400 MHz, $CDCl_3$): δ (ppm) 1.55 (t, J(PH) = 3.6 Hz, 36H, PMe_3), 1.58 (d, J(PH) = 3.6 Hz, 18H, PMe_3), 7.28(t, J (HH)= 9.6 Hz, 2H, Ar), 7.13-7.33(m, 2H, Ar-CH=), 7.39(d, J(HH) = 6 Hz, 2H, Ar), 7.71-7.75(m, 2H, Ru-CH=), 7.85(t, J(HH) = 9.6 Hz, 2H, Ar), 8.60(d, J(HH) = 7.2 Hz, 2H, Ar), 9.24(s, 2H, Ar). ^{13}C NMR (100 MHz, $CDCl_3$): δ (ppm) 17.45 (ppm) (t, J = 15.2 Hz, PMe_3), 20.07 (d, J = 20.6 Hz, PMe_3), 122.97, 124.11, 125.36, 127.42, 127.99, 128.24, 128.39, 129.96, 133.45, 135.78 (Ar-CH=), 170.82 (Ru-CH=), 202.47 (CO). ^{31}P NMR (160 MHz, $CDCl_3$): δ (ppm) -18.96 (ppm) (t, J = 22.56 Hz, PMe_3), -7.07 (d, J = 22.72 Hz, PMe_3). IR (KBr/cm^{-1}): ν(CO) 1914 (s); ν(C=C) 1555 (m). Anal. Calcd for $C_{42}H_{70}Cl_2O_2P_6Ru_2$: C, 47.33; H, 6.62. Found: C, 47.52; H, 6.49.

2. Crystallographic Information

Single crystals of complexes **3, 5** and **5d** suitable for X-ray analysis were obtained by slow diffusion of hexane into a solution of dichloromethane (CCDC number : 1992034; 1992052 and 1992053, respectively). Crystals with approximate dimensions of 0.16 × 0.15 × 0.10 mm^3 for **3**, 0.16 × 0.12 × 0.10 mm^3 for **5** and 0.16 × 0.12 × 0.10 mm^3 for **5d** were mounted on glass fibers for diffraction experiments. Intensity data were collected on a Nonius Kappa CCD diffractometer with Mo Kα radiation (λ_α = 0.71073 Å) at room temperature (298 K) or low temperature (100 K or 200K). The structures were solved by a combination of direct methods (SHELXS-97)[7] and Fourier difference techniques and refined by fullmatrix least squares (SHELXL-97)[8]. All non-H atoms were refined anisotropically. The hydrogen atoms were placed in ideal positions and refined as riding atoms. The partial solvent molecules have been omitted. Further crystal data and details of the data collection are summarized in Table S1.

Table S1. Crystal data and structure refinement for complexes **3**, **5** and **5d**

Complexes	**3**, CH_2Cl_2	**5**, $2CH_2Cl_2$	**5d**, CH_2Cl_2, Hexane
formula	$C_{39}H_{68}Cl_4O_2P_6Ru_2$	$C_{44}H_{72}Cl_6O_2P_6Ru_2$	$C_{39}H_{56}Cl_3OP_3Ru$
FW	1098.69	1235.76	841.16
Temperature	298.15 K	100.15 K	200.15 K
Wavelength	0.71073 Å	0.71073 Å	0.71073 Å
Crystal system	Monoclinic	Monoclinic	Monoclinic
Space group	C2/c	P2(1)/c	P2(1)/n
a(Å)	23.7595(11)	12.081(4)	12.6187(11)
b(Å)	14.4168(11)	13.350(4)	13.0122(12)
c(Å)	31.0806(18)	17.656(6)	25.898(2)
α(°)	90	90	90
β(°)	93.6870(10)	94.255(5)	96.0210(10)
γ(°)	90	90	90
V ($Å^3$)	10624.2(11)	2839.7(16)	4228.9(7)
Z	8	2	4
Density (calculated)(Mg/m^3)	1.374	1.443	1.321
Absorption coefficient(mm^{-1})	0.979	1.016	0.702
F(000)	4512	1264	1752
Crystal size (mm^3)	0.16 x 0.15 x 0.10	0.16 x 0.12 x 0.10	0.16 x 0.12 x 0.10
θ Range (°)	1.799 to 26.498	1.690 to 24.999	1.753 to 24.999
Index ranges	-29<=h<=29, -18<=k<=18, -39<=l<=39	-14<=h<=14, -15<=k<=15, -20<=l<=20	-15<=h<=12, -15<=k<=15, -30<=l<=30
Reflections collected	56905	19432	27161
Independent reflec.	10979 [R(int) = 0.0542]	4971 [R(int) = 0.0586]	7408 [R(int) = 0.0235]
Refinement method	Full-matrix least-squares on F^2	Full-matrix least-squares on F^2	Full-matrix least-squares on F^2
Data / restraints / parameters	10979 / 0 / 558	4971 / 60 / 380	7408 / 9 / 435
Goodness-of-fit on F^2	1.051	1.388	1.045
Final R indices [I>2sigma(I)]	R1 = 0.0366, wR2 = 0.1007	R1 = 0.1141, wR2 = 0.3160	R1 = 0.0468, wR2 = 0.1367
R indices (all data)	R1 = 0.0455, wR2 = 0.1051	R1 = 0.1580, wR2 = 0.2402	R1 = 0.0528, wR2 = 0.1468

Largest diff. peak and hole	0.858 and -0.446 e.Å^{-3}	4.247 and -1.318 e.Å^{-3}	1.029 and -1.236 e.Å^{-3}

Table S2. Selected Bond Lengths(Å), Angles(deg) and Dihedral Angles(deg) from Crystal Structure of **5** and the DFT-Optimized Structures [**5**−**H**]$^{n+}$(*n* = 0, 1, 2)

	5	[**5**−**H**]	[**5**−**H**]$^{+}$	[**5**−**H**]$^{2+}$
Bond Lengths (Å)				
Ru(1)-P(2)	2.395(3)	2.439	2.455	2.495
Ru(1)-C(30)	2.16(3)	2.109	2.081	2.019
C(30)-C(29)	1.21(3)	1.345	1.362	1.396
C(29)-C(22)	1.523(9)	1.491	1.460	1.413
C(22)-C(23)	1.401(8)	1.407	1.433	1.456
C(23)-C(28)	1.390(0)	1.459	1.445	1.433
C(28)-C(21)	1.397(8)	1.407	1.433	1.456
C(22)-C(19)	1.413(9)	1.428	1.442	1.462
C(19)-C(18)	1.406(8)	1.453	1.454	1.454
C(18)-C(21)	1.412(8)	1.428	1.442	1.462
C(21)-C(31)	1.522(9)	1.491	1.460	1.413
C(31)-C(32)	1.224(18)	1.345	1.362	1.396
Bond Angles (deg)				
P(1)-Ru(1)-P(3)	167.80(10)	162.56	166.93	169.52
P(2)-Ru(1)-C(30)	176.7(6)	169.94	169.66	169.51
Ru(1)-C(30)-C(29)	127.6(16)	129.87	130.11	131.98
C(30)-C(29)-C(22)	127.8(17)	124.71	125.73	126.57
C(21)-C(31)-C(32)	131(2)	124.71	125.73	126.57
Dihedral Angles (deg)				
Plane[Ru(1), C(30), C(29)] Plane[C(22), C(19), C(18)]	57.74	58.33	41.01	21.55
Plane[C(19), C(18), C(21)] Plane[C(31), C(32), Ru(1)]	43.13	55.59	41.01	21.56
Plane[Ru(1), C(30), C(29)] Plane[C(31), C(32), Ru(1)]	16.11	66.29	76.25	45.81

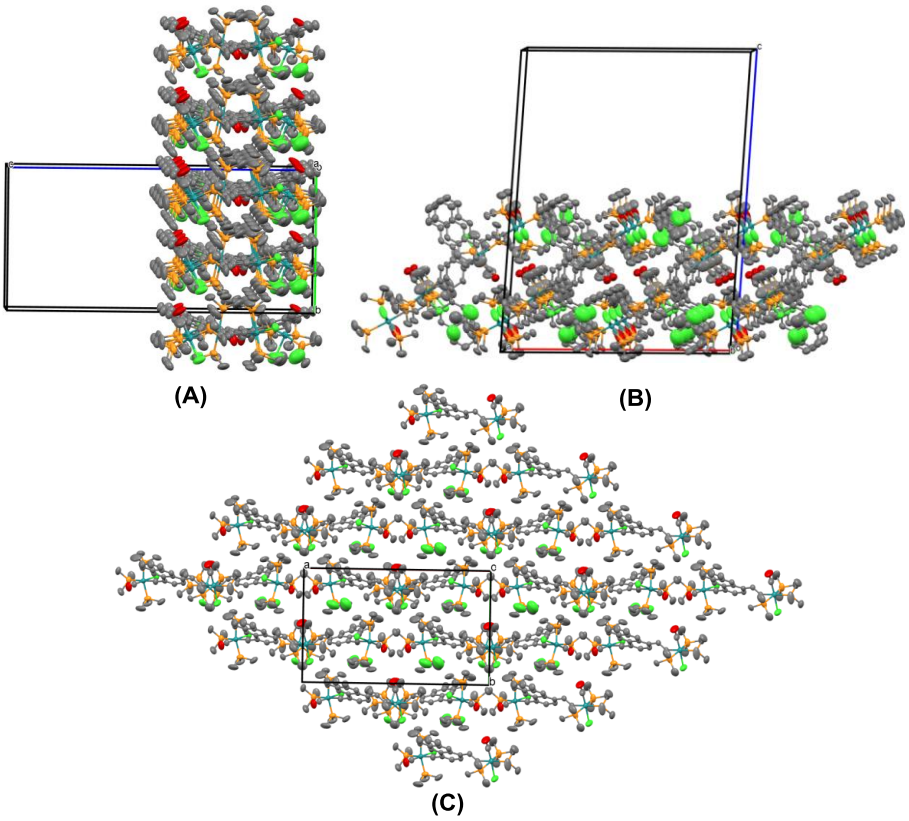

Figure S1. Packing diagram of complex **3**. Packing viewing along axis *a* (A), *b* (B) and *c* (C) respectively.

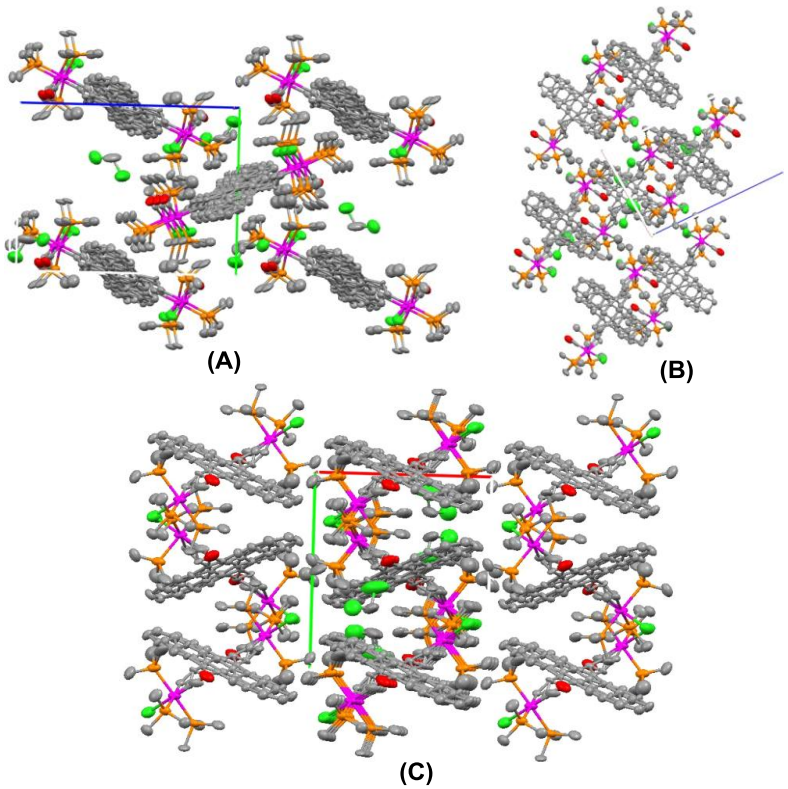

Figure S2. Packing diagram of complex **5**. Packing viewing along axis *a* (A), *b* (B) and *c* (C) respectively.

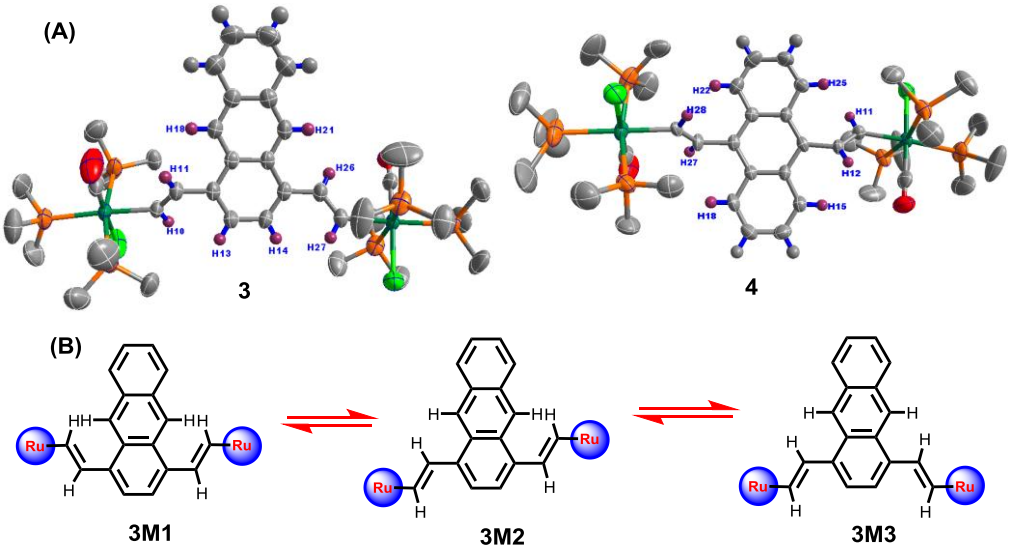

Figure S3. The crystal structures of complexes **3** and **4** with adjacent hydrogen atoms have been marked under top viewing (A) and three representative molecular configurations of complex **3**.

3. UV–Vis–NIR Spectral Information

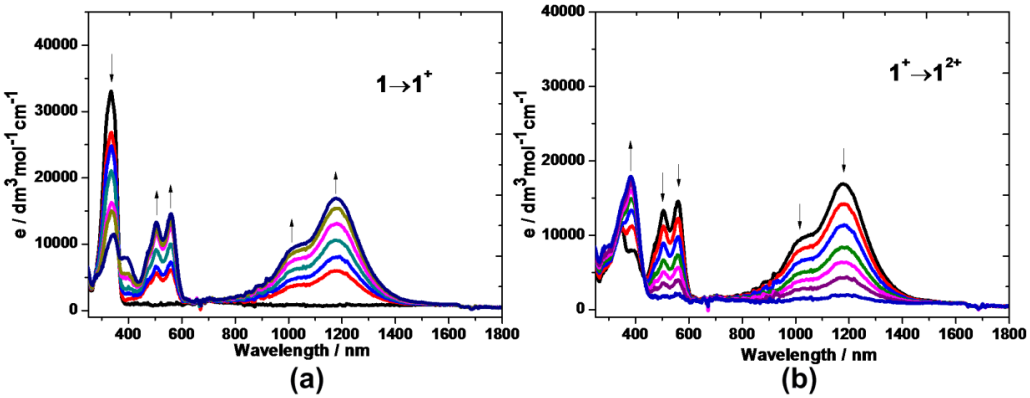

Figure S4. UV–vis–NIR spectral changes recorded during the oxidation $\mathbf{1}\rightarrow\mathbf{1}^{+}$ (a) and $\mathbf{1}^{+}\rightarrow\mathbf{1}^{2+}$ (b) in CH_2Cl_2 / 10^{-1} M $^{n}Bu_4NPF_6$ at 298 K within a OTTLE cell.

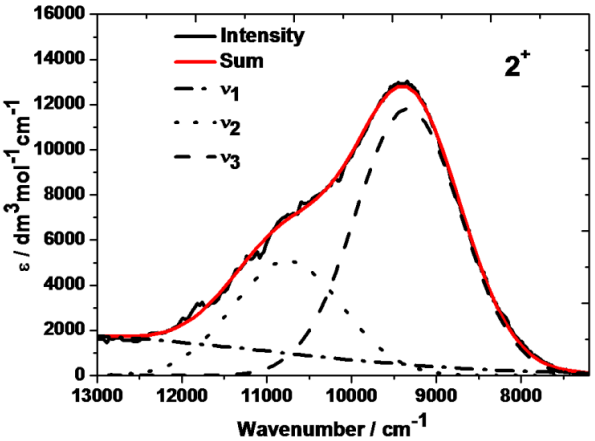

Figure S5. NIR region of the electronic spectrum of $\mathbf{2}^{+}$ showing deconvolution into a

sum of three Gaussian-shaped bands.

4. DFT Calculations

DFT calculations were performed with the Gaussian 09 programs.[9] Simplified model complexes **[1–H]**^{n}–**[5–H]**$^{n+}$ (n = 0, 1, 2) were optimized at the B3LYP/3-21G* level of theory. Geometry optimizations were performed without any symmetry constraints. Electronic transitions were calculated by the time-dependent DFT (TDDFT) method based on full-optimized structures **[1]**$^{n+}$–**[5]**$^{n+}$ (n = 0, 1) on the (U)B3LYP/LANL2DZ/6-31G*/CPCM level of theory.[10] Nucleus independent chemical shift (NICS) calculations[11] (GAIO-B3LYP/LANL2DZ/6-31G*) based on the full-optimized structures. The MO contributions and π-conjugation orbital diagram were generated using the Multiwfn_3.7_dev_bin_Win64 and plotted using GaussView 5.0 or Multiwfn program.

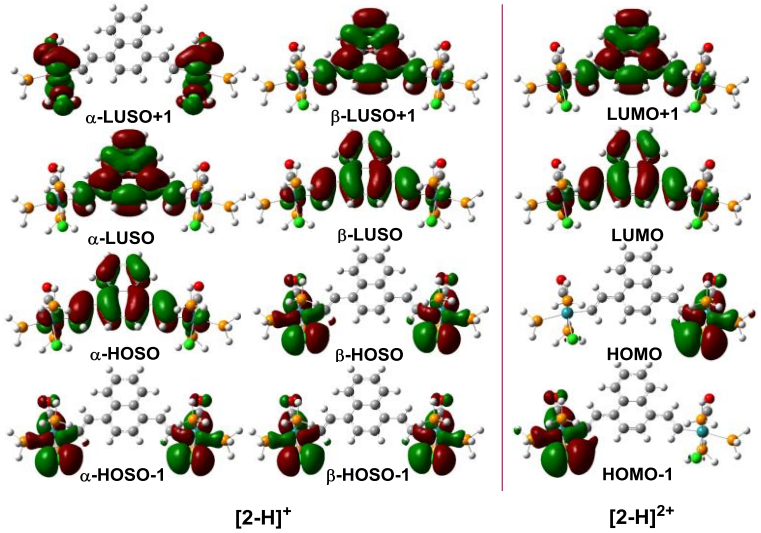

Figure S6. Selected frontier molecular orbitals from complexes [**2**−**H**]$^{+}$ and [**2**−**H**]$^{2+}$ plotted with contour values ±0.04 (e/bohr^{3})$^{1/2}$

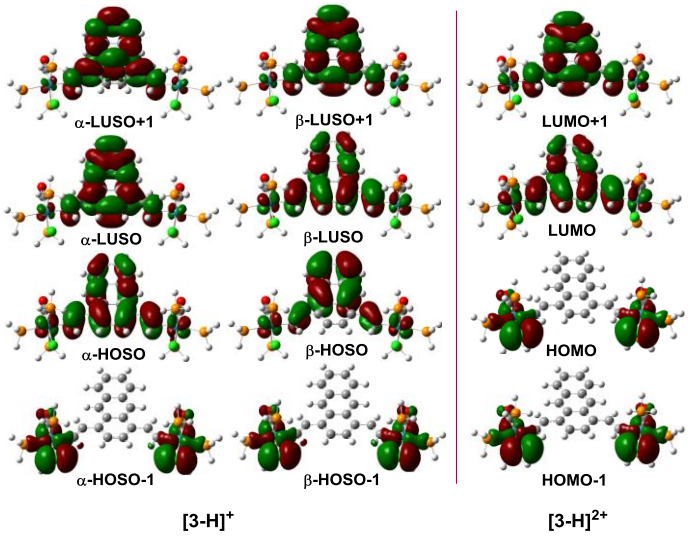

Figure S7. Selected frontier molecular orbitals from complexes [**3**−**H**]$^{+}$ and [**3**−**H**]$^{2+}$ plotted with contour values ±0.04 (e/bohr^{3})$^{1/2}$

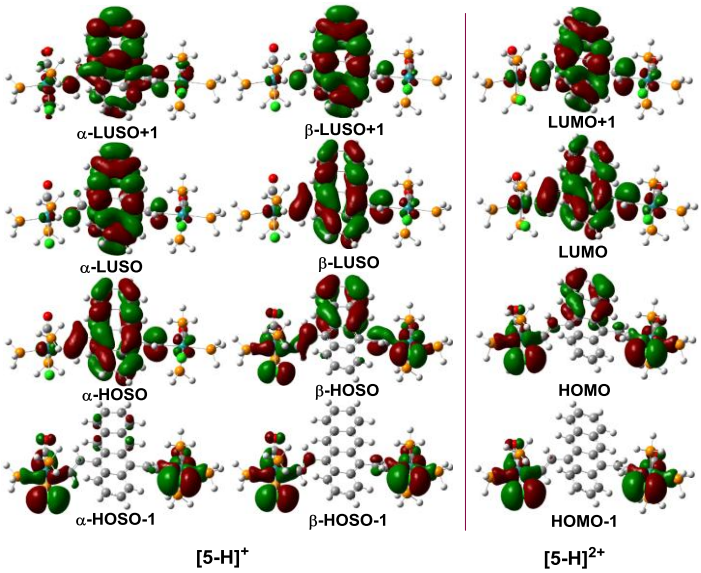

Figure S8. Selected frontier molecular orbitals from complexes $[\mathbf{5-H}]^{+}$ and $[\mathbf{5-H}]^{2+}$ plotted with contour values ±0.04 $(e/bohr^3)^{1/2}$

Table S3. Energy and composition of frontier molecular orbitals in the model complexes **[2−H]**

MO	Orbitals	eV	(CO)1	Cl1	$(PH_3)_3$1	Ru1	(C=C)1	$C_{10}H_6$	(C=C)2	Ru2	$(PH_3)_3$2	Cl2	(CO)2
182	L+5	-0.30	27	1	1	19	1	0	1	19	1	1	27
181	L+4	-0.55	9	1	14	24	2	0	2	24	14	1	9
180	L+3	-0.55	8	1	14	24	2	0	2	24	14	1	8
179	L+2	-1.01	4	5	10	29	1	0	1	28	10	5	4
178	L+1	-1.01	4	5	11	29	0	0	0	30	11	5	4
177	LUMO	-0.11	1	1	3	4	10	62	10	4	3	1	1
176	HOMO	-4.95	0	0	1	5	15	58	15	5	1	0	0
175	H-1	-6.21	0	6	1	20	19	8	19	20	1	6	0
174	H-2	-6.28	3	27	2	16	3	1	3	15	2	25	3
173	H-3	-6.28	2	24	2	14	3	7	3	15	2	26	2
172	H-4	-6.34	2	24	3	14	1	11	2	14	3	24	2
171	H-5	-6.40	0	3	0	2	0	90	0	2	0	3	0

Table S4. Energy and composition of frontier molecular orbitals in the model complexes $\mathbf{[2-H]^{+}}$

MO	Orbitals	eV	(CO)1	Cl1	$(PH_3)_3$1	Ru1	(C=C)1	$C_{10}H_6$	(C=C)2	Ru2	$(PH_3)_3$2	Cl2	(CO)2
182α	α-LUSO+5	-3.09	0	0	0	1	3	90	3	1	0	0	0
181β	β-LUSO+5	-3.11	13	1	10	23	2	0	2	23	10	1	13
181α	α-LUSO+4	-3.12	12	1	10	23	2	0	2	23	10	1	12
180β	β-LUSO+4	-3.12	13	1	10	22	2	0	2	22	10	1	13
180α	α-LUSO+3	-3.13	13	1	10	23	2	0	2	23	10	1	13
179β	β-LUSO+3	-3.56	3	5	12	29	1	0	1	28	12	5	3
179α	α-LUSO+2	-3.59	3	5	12	29	1	0	1	28	12	5	3
178β	β-LUSO+2	-3.56	3	5	12	28	1	0	1	29	12	5	3

178α	α-LUSO+1	-3.59	3	5	12	28	1	0	1	29	12	5	3
177β	β-LUSO+1	-4.35	0	0	1	4	15	60	15	4	1	0	0
177α	α-LUSO	-4.83	0	0	1	3	15	62	15	3	1	0	0
176β	β-LUSO	-6.68	0	0	1	6	19	48	19	6	1	0	0
176α	α-HOSO	-7.99	0	0	1	9	19	42	19	9	1	0	0
175β	β-HOSO	-8.83	2	31	2	14	1	0	1	14	2	31	2
175α	α-HOSO-1	-8.84	2	32	2	13	1	0	1	13	2	32	2
174β	β-HOSO-1	-8.83	2	31	2	14	1	0	1	14	2	32	2
174α	α-HOSO-2	-8.84	2	32	2	13	1	0	1	13	2	32	2
173β	β-HOSO-2	-8.86	1	22	1	17	7	4	7	17	1	22	1
173α	α-HOSO-3	-8.90	2	36	2	11	0	0	0	11	2	36	2
172β	β-HOSO-3	-8.89	2	36	2	11	0	0	0	11	2	36	2
172α	α-HOSO-4	-8.90	2	36	2	11	0	0	0	11	2	36	2
171β	β-HOSO-4	-8.95	1	14	3	16	12	8	12	16	3	14	1
171α	α-HOSO-5	-9.25	0	1	3	25	16	10	16	25	3	1	0
170β	β-HOSO-5	-9.34	0	1	1	16	5	54	5	16	1	1	0

Table S5. Energy and composition of frontier molecular orbitals in the model complexes **[2−H]**$^{2+}$

MO	Orbitals	eV	(CO)1	Cl1	$(PH_3)_3$1	Ru1	(C=C)1	$C_{10}H_6$	(C=C)2	Ru2	$(PH_3)_3$2	Cl2	(CO)2
181	L+5	-5.86	18	2	9	23	1	0	1	20	8	2	16
180	L+4	-5.99	0	0	0	1	6	86	6	1	0	0	0
179	L+3	-6.36	2	4	15	25	0	0	0	29	17	5	2
178	L+2	-6.36	2	5	17	29	0	0	0	25	15	4	2
177	L+1	-7.79	0	0	1	5	17	54	17	5	1	0	0
176	LUMO	-9.74	0	0	1	9	19	42	19	9	1	0	0
175	HOMO	-11.5	0	1	0	0	0	0	0	21	3	71	3
174	H-1	-11.5	3	71	3	21	0	0	0	0	0	1	0
173	H-2	-11.5	0	0	0	0	0	0	0	18	4	76	3
172	H-3	-11.5	3	76	4	18	0	0	0	0	0	0	0
171	H-4	-11.9	0	0	2	22	15	22	15	22	2	0	0
170	H-5	-12.3	0	0	0	12	4	68	4	12	0	0	0

Table S6. Energy and composition of frontier molecular orbitals in the model complexes **[3−H]**

MO	Orbitals	eV	(CO)1	Cl1	$(PH_3)_3$1	Ru1	(C=C)1	$C_{14}H_8$	(C=C)2	Ru2	$(PH_3)_3$2	Cl2	(CO)2
195	L+5	-0.38	15	0	1	14	6	28	6	14	1	0	15
194	L+4	-0.56	9	0	12	25	2	0	2	25	12	0	9
193	L+3	-0.57	9	0	12	24	2	0	2	24	12	0	9
192	L+2	-1.03	4	5	11	31	0	0	0	28	11	5	4
191	L+1	-1.03	4	5	11	28	0	0	0	31	11	5	4
190	LUMO	-1.54	0	0	1	1	5	86	5	1	1	0	0
189	HOMO	-4.77	0	0	1	3	10	72	10	3	1	0	0

188	H-1	-5.87	0	1	0	7	13	58	13	7	0	1	0
187	H-2	-6.23	1	6	1	20	19	6	19	20	1	6	1
186	H-3	-6.29	2	24	2	14	3	10	3	14	2	23	2
185	H-4	-6.30	3	28	2	15	2	0	2	15	2	28	3
184	H-5	-6.37	1	4	0	2	0	86	0	2	0	4	1

Table S7. Energy and composition of frontier molecular orbitals in the model complexes **[3−H]$^{+}$**

MO	Orbitals	eV	(CO)1	Cl1	$(PH_3)_3$1	Ru1	(C=C)1	$C_{14}H_8$	(C=C)2	Ru2	$(PH_3)_3$2	Cl2	(CO)2
195α	α-LUSO+5	-3.02	12	1	10	23	2	0	2	23	10	1	12
194β	β-LUSO+5	-3.01	12	1	10	23	2	0	0	23	10	1	12
194α	α-LUSO+4	-3.07	0	0	0	1	2	94	2	1	0	0	0
193β	β-LUSO+4	-3.31	0	0	1	3	13	66	13	3	1	0	0
193α	α-LUSO+3	-3.47	3	5	12	28	0	0	0	28	12	5	3
192β	β-LUSO+3	-3.46	3	5	12	28	0	0	0	28	12	5	3
192α	α-LUSO+2	-3.47	3	5	12	28	0	0	0	28	12	5	3
191β	β-LUSO+2	-3.46	3	5	12	28	0	0	0	28	12	5	3
191α	α-LUSO+1	-3.54	0	0	1	2	12	70	12	2	1	0	0
190β	β-LUSO+1	-4.59	0	0	1	2	9	76	9	2	1	0	0
190α	α-LUSO	-5.02	0	0	1	2	9	76	9	2	1	0	0
189β	β-LUSO	-6.50	0	0	1	5	16	56	16	5	1	0	0
189α	α-HOSO	-7.73	0	0	1	6	15	56	15	6	1	0	0
188β	β-HOSO	-8.53	0	1	0	6	7	72	7	6	0	1	0
188α	α-HOSO-1	-8.73	2	32	2	14	1	0	1	14	2	32	2
187β	β-HOSO-1	-8.73	2	31	2	14	1	0	1	14	2	31	2
187α	α-HOSO-2	-8.74	2	32	1	14	1	0	1	14	1	32	2
186β	β-HOSO-2	-8.73	2	31	1	14	1	0	1	14	1	31	2
186α	α-HOSO-3	-8.77	1	11	0	10	5	46	5	10	0	11	1
185β	β-HOSO-3	-8.77	2	29	1	14	4	0	4	14	1	29	2
185α	α-HOSO-4	-8.80	2	36	2	11	0	0	0	11	2	36	2
184β	β-HOSO-4	-8.79	2	36	2	11	0	0	0	11	2	36	2
184α	α-HOSO-5	-8.81	1	25	2	9	3	20	3	9	2	25	1
183β	β-HOSO-5	-8.89	1	8	2	18	15	12	15	18	2	8	1

Table S8. Energy and composition of frontier molecular orbitals in the model complexes **[3−H]$^{2+}$**

MO	Orbitals	eV	(CO)1	Cl1	$(PH_3)_3$1	Ru1	(C=C)1	$C_{14}H_8$	(C=C)2	Ru2	$(PH_3)_3$2	Cl2	(CO)2
194	L+5	-5.84	0	0	0	1	2	94	2	1	0	0	0
193	L+4	-6.10	2	5	14	27	1	0	1	27	14	5	2
192	L+3	-6.10	2	5	14	27	1	0	1	27	14	5	2
191	L+2	-6.35	0	0	0	2	12	72	12	2	0	0	0
190	L+1	-7.83	0	0	1	4	12	66	12	4	1	0	0
189	LUMO	-9.46	0	0	1	7	16	52	16	7	1	0	0

188	HOMO	-11.2	2	35	2	11	1	0	1	11	2	35	2
187	H-1	-11.2	2	35	2	11	1	0	1	11	2	35	2
186	H-2	-11.3	3	71	3	17	0	0	0	1	0	5	0
185	H-3	-11.3	0	5	0	1	0	0	0	17	3	71	3
184	H-4	-11.3	0	0	1	6	5	76	5	6	1	0	0
183	H-5	-11.7	0	0	2	22	14	24	14	22	2	0	0

Table S9. Energy and composition of frontier molecular orbitals in the model complexes **[5−H]**

MO	Orbitals	eV	(CO)1	Cl1	$(PH_3)_3$1	Ru1	(C=C)1	$C_{14}H_8$	(C=C)2	Ru2	$(PH_3)_3$2	Cl2	(CO)2
208	L+5	-0.38	21	1	0	17	2	18	2	17	0	1	21
207	L+4	-0.61	9	1	13	27	3	4	3	21	10	1	8
206	L+3	-0.61	8	1	10	21	3	4	3	27	13	1	9
205	L+2	-1.06	4	6	10	32	0	0	0	27	9	5	4
204	L+1	-1.06	4	5	9	27	0	0	0	32	10	6	4
203	LUMO	-1.89	0	0	0	1	2	94	2	1	0	0	0
202	HOMO	-4.55	0	0	0	1	4	90	4	1	0	0	0
201	H-1	-5.95	0	0	0	5	11	68	11	5	0	0	0
200	H-2	-6.21	0	3	1	19	23	8	23	19	1	3	0
199	H-3	-6.30	1	7	1	5	2	68	2	5	1	7	1
198	H-4	-6.31	2	27	2	15	3	0	3	15	2	27	2
197	H-5	-6.33	2	21	1	11	2	26	2	11	1	21	2

Table S10. Energy and composition of frontier molecular orbitals in the model complexes **[5−H]**$^+$

MO	Orbitals	eV	(CO)1	Cl1	$(PH_3)_3$1	Ru1	(C=C)1	$C_{14}H_8$	(C=C)2	Ru2	$(PH_3)_3$2	Cl2	(CO)2
208α	α-LUSO+5	-2.95	9	1	9	20	2	2	3	25	12	1	11
207β	β-LUSO+5	-3.11	0	0	1	1	1	94	1	1	1	0	0
207α	α-LUSO+4	-3.19	0	0	1	1	1	94	1	1	1	0	0
206β	β-LUSO+4	-3.25	1	1	3	7	5	66	5	7	3	1	1
206α	α-LUSO+3	-3.34	4	4	10	26	1	8	1	26	10	4	4
205β	β-LUSO+3	-3.35	4	5	10	28	1	0	1	28	10	5	4
205α	α-LUSO+2	-3.36	4	5	10	28	1	0	1	28	10	5	4
204β	β-LUSO+2	-3.37	4	4	9	23	2	0	2	23	9	4	4
204α	α-LUSO+1	-3.48	1	1	1	3	6	76	6	3	1	1	1
203β	β-LUSO+1	-4.86	0	0	0	1	5	88	5	1	0	0	0
203α	α-LUSO	-5.31	0	0	0	1	5	88	5	1	0	0	0
202β	β-LUSO	-6.40	0	0	1	2	9	76	9	2	1	0	0
202α	α-HOSO	-7.59	0	0	1	4	10	70	10	4	1	0	0
201β	β-HOSO	-8.54	1	12	1	11	6	38	6	11	1	12	1
201α	α-HOSO-1	-8.60	2	30	1	13	2	2	2	13	1	30	2
200β	β-HOSO-1	-8.59	2	29	1	15	3	0	3	15	1	29	2
200α	α-HOSO-2	-8.60	2	31	1	14	2	0	2	14	1	31	2
199β	β-HOSO-2	-8.64	1	21	1	10	5	24	5	10	1	21	1

199α	α-HOSO-3	-8.69	2	35	2	11	0	0	0	11	2	36	2
198β	β-HOSO-3	-8.69	2	35	2	11	0	0	0	11	2	35	2
198α	α-HOSO-4	-8.70	2	36	2	11	0	0	0	11	2	35	2
197β	β-HOSO-4	-8.69	2	35	2	10	0	0	0	10	2	35	2
197α	α-HOSO-5	-8.80	0	3	1	9	9	56	9	9	1	3	0
196β	β-HOSO-5	-8.85	0	4	1	21	17	14	17	21	1	4	0

Table S11. Energy and composition of frontier molecular orbitals in the model complexes **[5−H]**$^{2+}$

MO	Orbitals	eV	(CO)1	Cl1	$(PH_3)_3$1	Ru1	(C=C)1	$C_{14}H_8$	(C=C)2	Ru2	$(PH_3)_3$2	Cl2	(CO)2
207	L+5	-5.91	1	1	6	10	2	60	2	10	6	1	1
206	L+4	-5.94	2	4	13	24	1	10	1	24	13	4	2
205	L+3	-5.97	2	4	8	18	2	32	2	18	8	4	2
204	L+2	-6.27	0	0	1	2	11	72	11	2	1	0	0
203	L+1	-7.99	0	0	1	3	11	70	11	3	1	0	0
202	LUMO	-9.02	0	0	1	5	14	60	14	5	1	0	0
201	HOMO	-11.1	1	24	2	10	2	22	2	10	2	24	1
200	H-1	-11.1	2	34	2	11	0	0	0	11	2	34	2
199	H-2	-11.2	1	38	2	9	0	0	0	9	2	37	1
198	H-3	-11.2	1	37	2	9	0	0	0	9	2	38	1
197	H-4	-11.2	1	12	0	7	5	50	5	7	0	12	1
196	H-5	-11.6	0	2	1	20	13	28	13	20	1	2	0

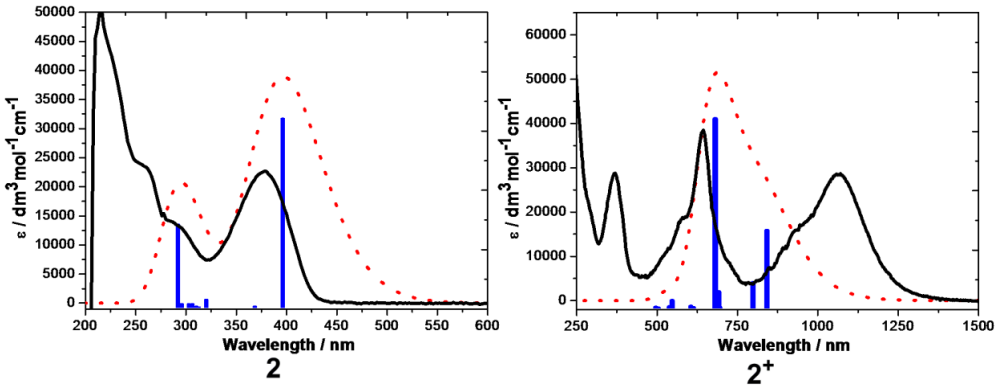

Figure S9. Electronic absorption spectra (black curves) and TDDFT-predicted singlet excitations (blue vertical lines and red dotted curves) of **2** and **2**$^{+}$

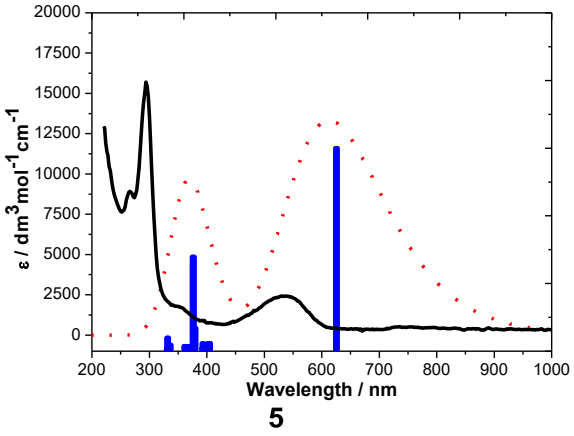

Figure S10. Electronic absorption spectra (black curves) and TDDFT-predicted singlet excitations (blue vertical lines and red dotted curves) of **5**

Table S12. Major electronic excitations for full-optimized structures **[2]**, **[3]** and **[5]** determined by TDDFT methods.

Complex	Wavelength (nm)	Osc. str (f)	Major contributions	Main assignement
[2]	397	0.9549	HOMO-LUMO (98%)	Bridge π-π* with a little mixture of MLCT
	293	0.4195	HOMO-LUMO+6 (88%)	Bridge π-π*
[3]	500	0.4111	HOMO-LUMO (99%)	Bridge π-π*with a little mixture of MLCT
	332	0.7113	HOMO-LUMO+4 (56%)	Bridge π-π*
[5]	613	0.3287	HOMO-LUMO (100%)	Bridge π-π*with a little mixture of MLCT
	369	0.1518	HOMO-LUMO+3 (76%)	Bridge π-π*

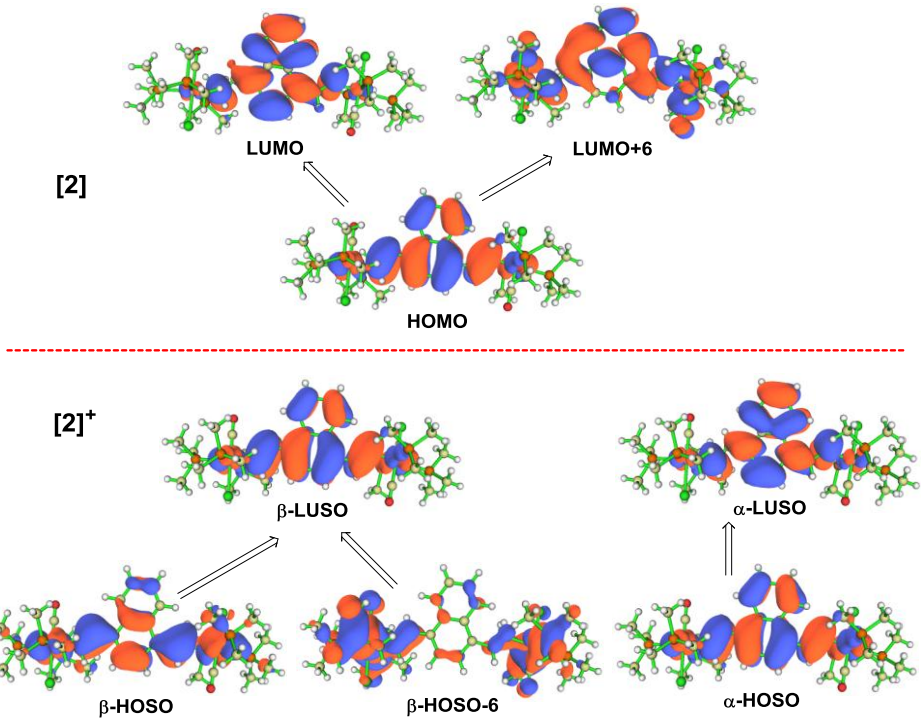

Figure S11. Isosurface plots of molecular orbitals involved in the major electronic excitations for neutral molecule [**2**] and singly-oxidized state [**2**]$^{+}$. Contour values: ±0.04 (e/bohr^{3})$^{1/2}$.

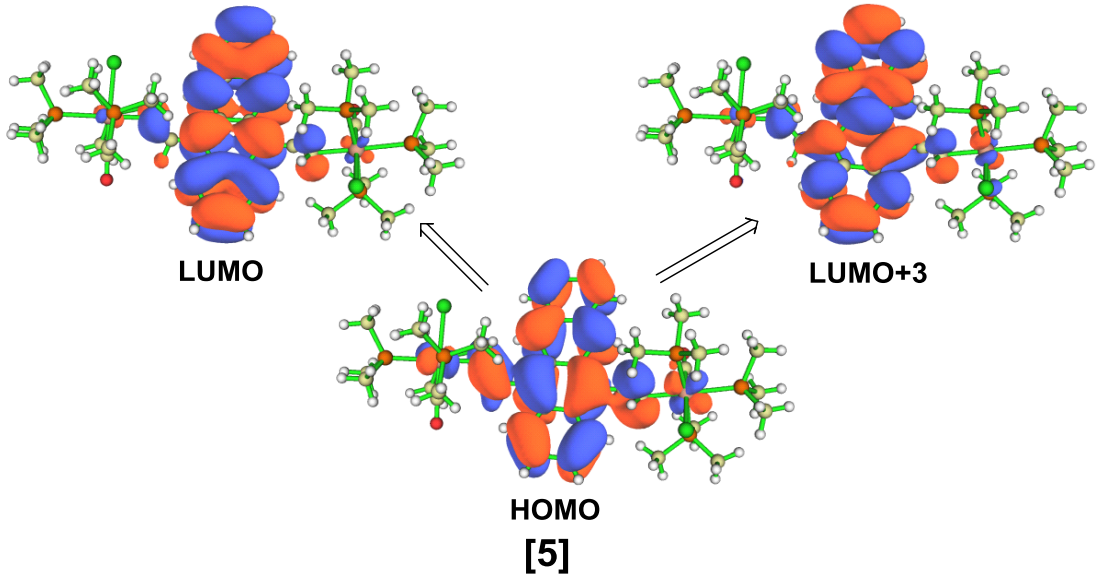

Figure S12. Isosurface plots of molecular orbitals involved in the major electronic excitations for neutral molecule [**5**]. Contour values: ±0.04 (e/bohr^{3})$^{1/2}$.

5. NICS(1)$_{zz}$ calculation and π-conjugation analysis

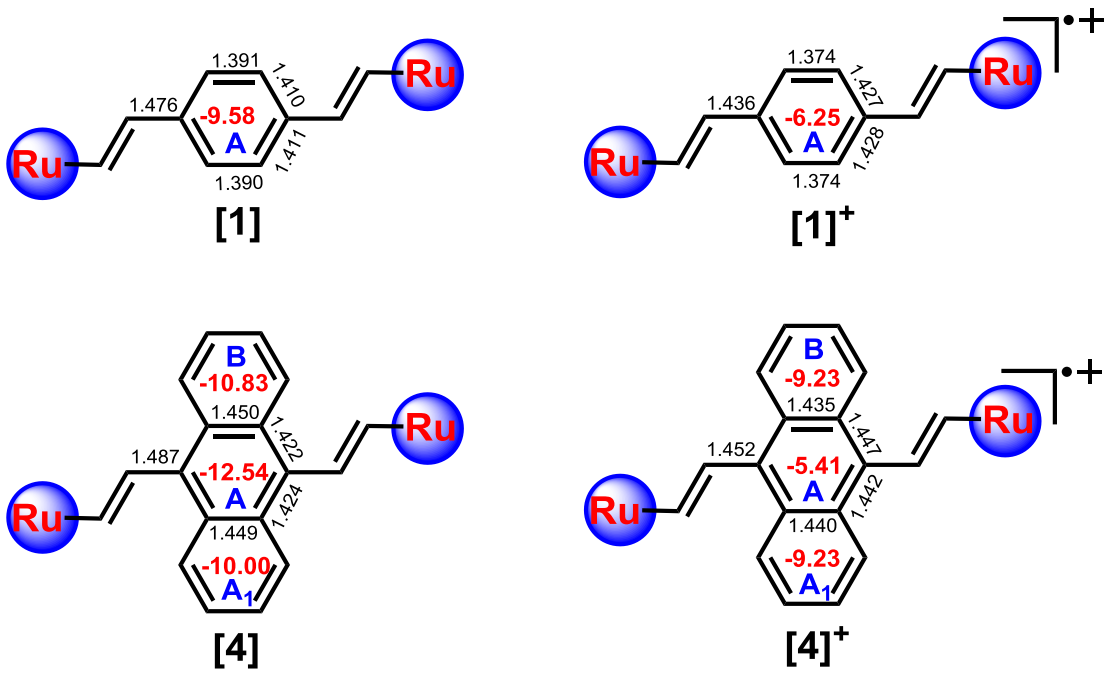

Figure S13. The calculated NICS(1)$_{zz}$ values (red font) for full-optimized complexes [**1**]$^{n+}$ and [**4**]$^{n+}$ (n = 0, 1) and selected bond length (Å) (black font) of rutheniumvinyl-substituted benzene ring, in which the rings are labeled by blue letters A, B and A_1, respectively.

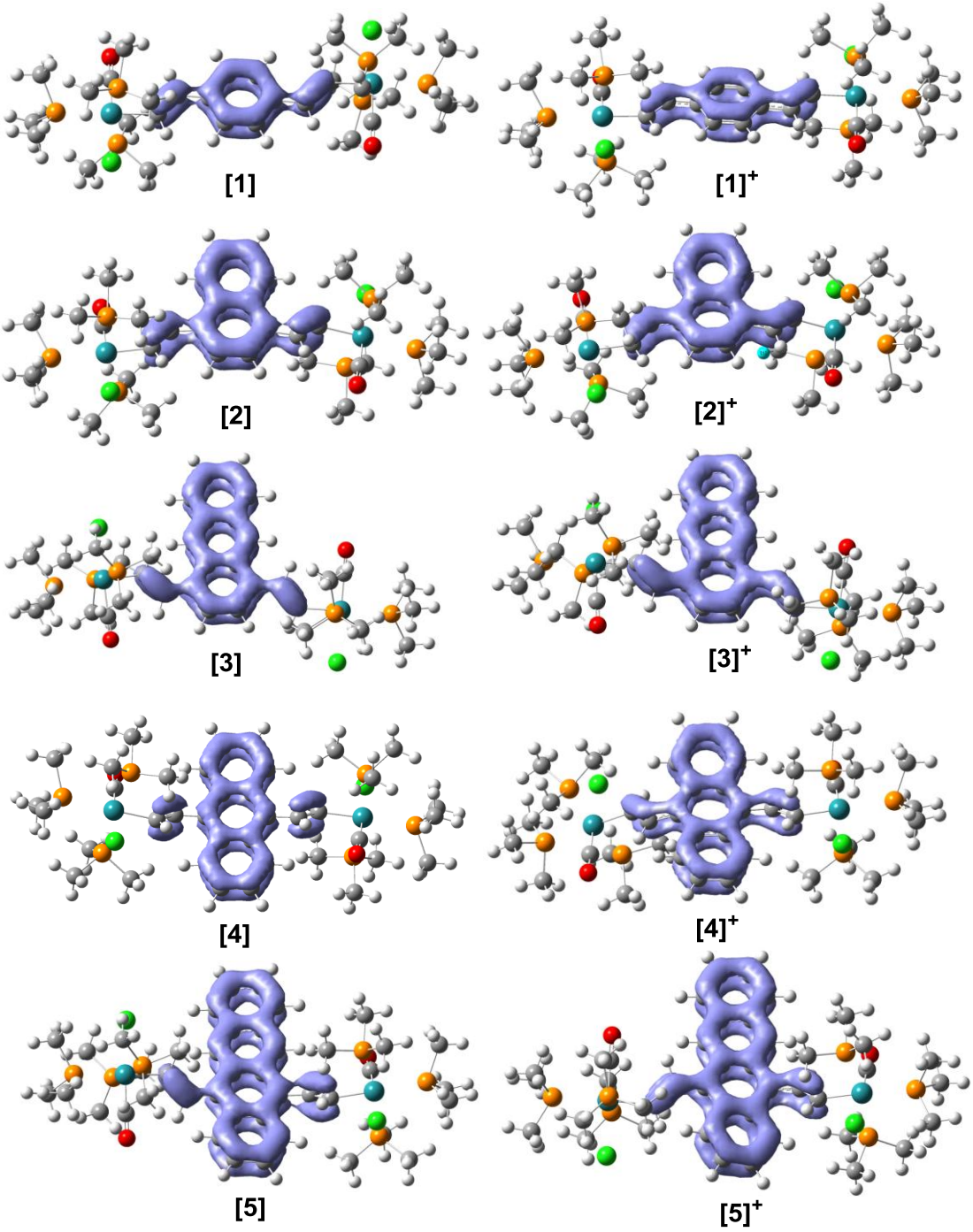

Figure S14. π-electron density distribution of full-optimized complexes **[1]**$^{n+}$–[5]$^{n+}$ (n = 0, 1) based on localized orbital locator (LOL) analysis

6. NMR Information

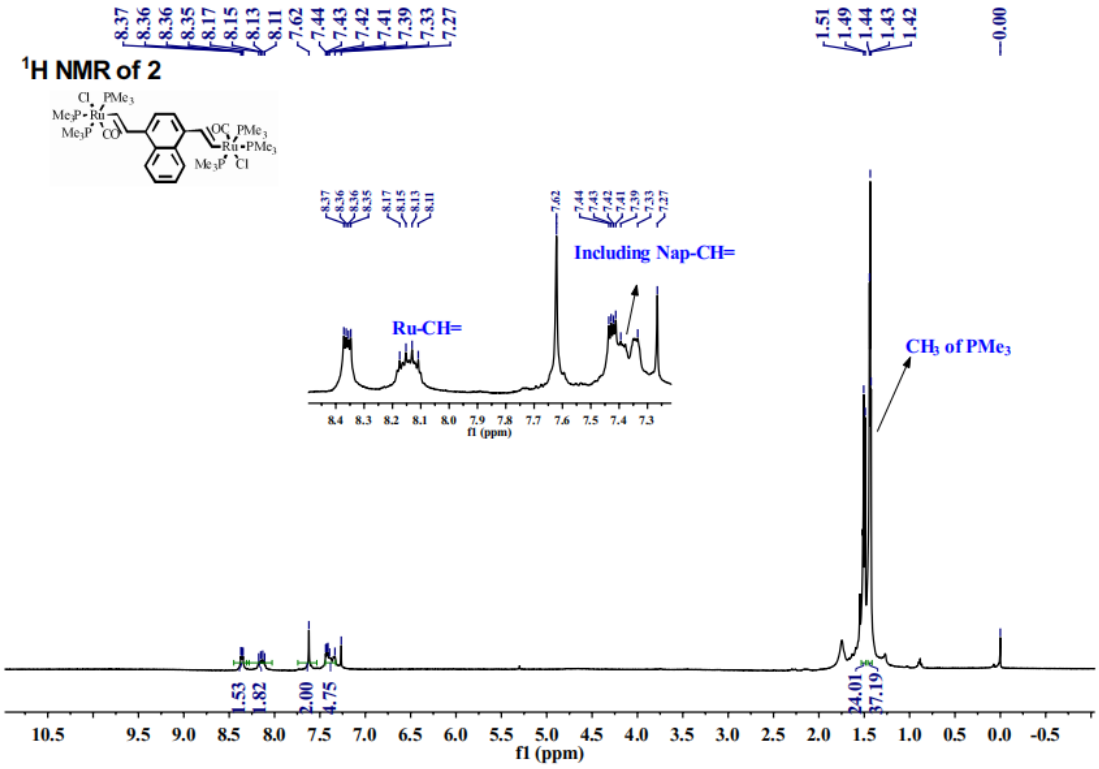

Figure S15. ^{1}H NMR spectrum (400 MHz, $CDCl_3$) of **2**.

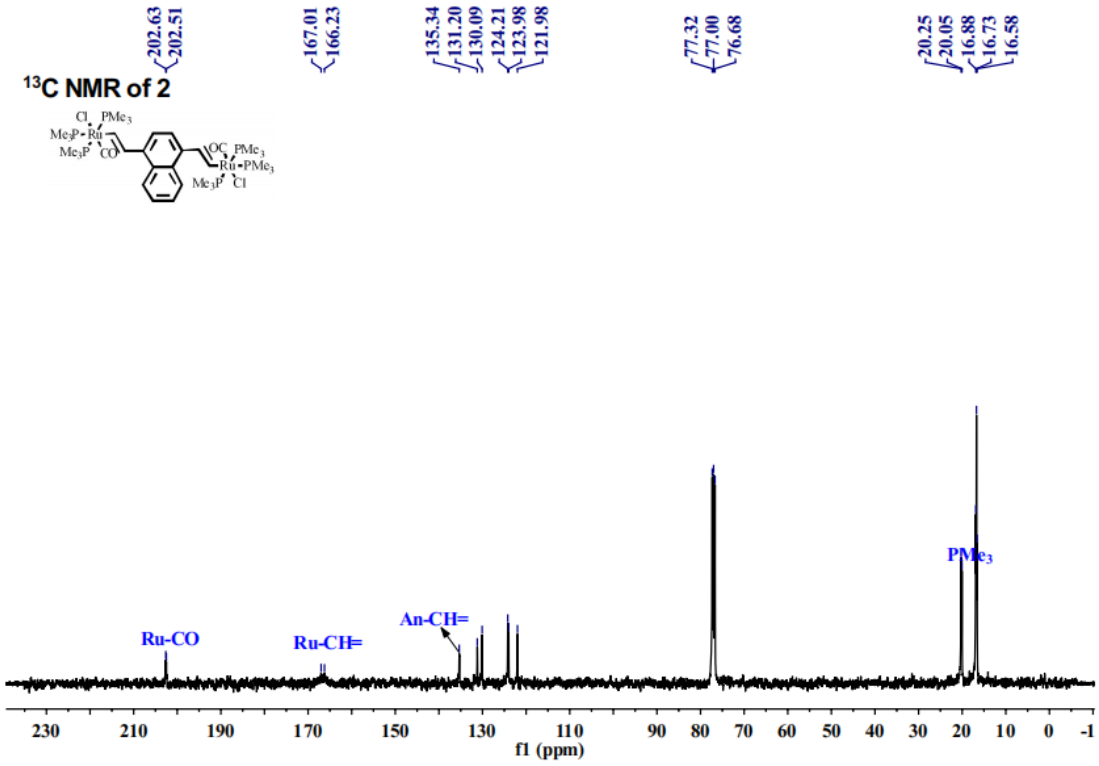

Figure S16. ^{13}C NMR spectrum (100 MHz, $CDCl_3$) of **2**.

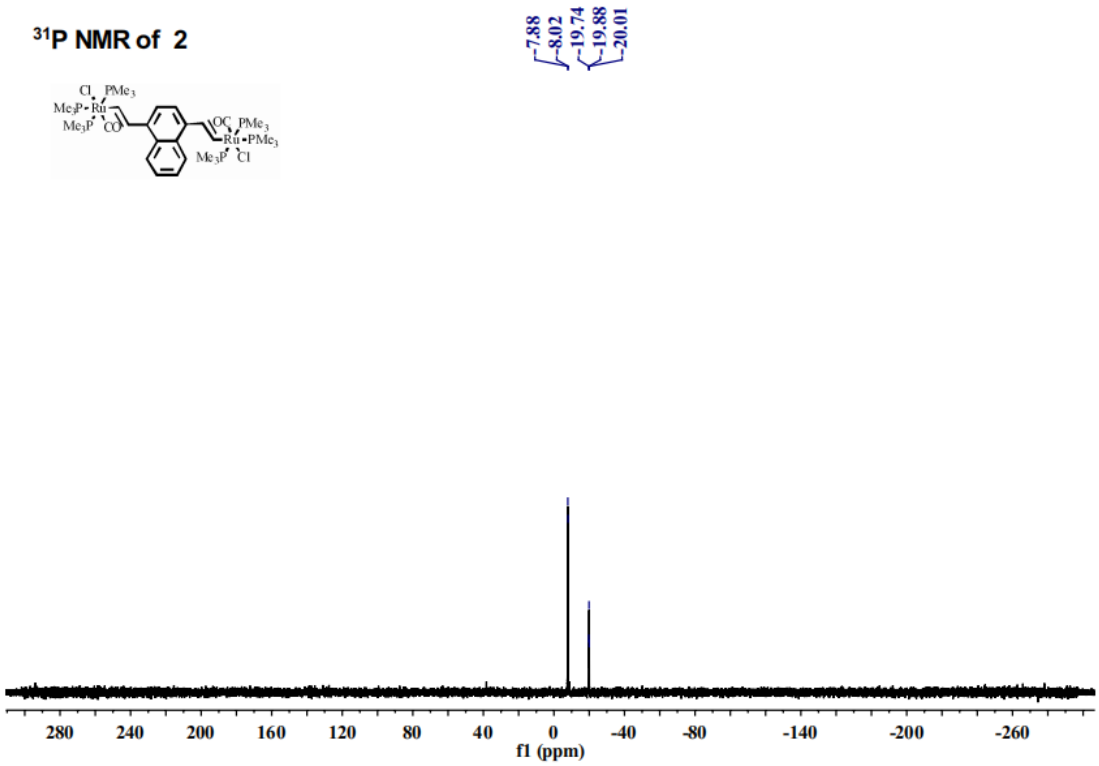

Figure S17. ^{31}P NMR spectrum (160 MHz, $CDCl_3$) of **2**.

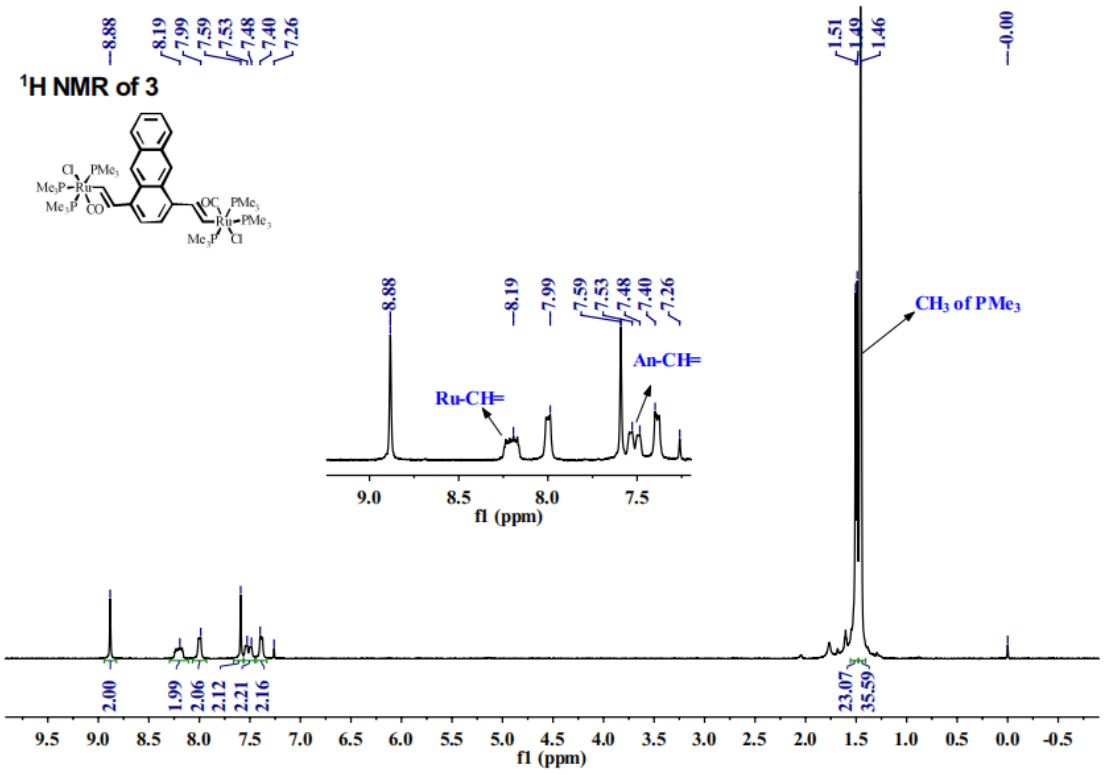

Figure S18. ^{1}H NMR spectrum (400 MHz, $CDCl_3$) of **3**.

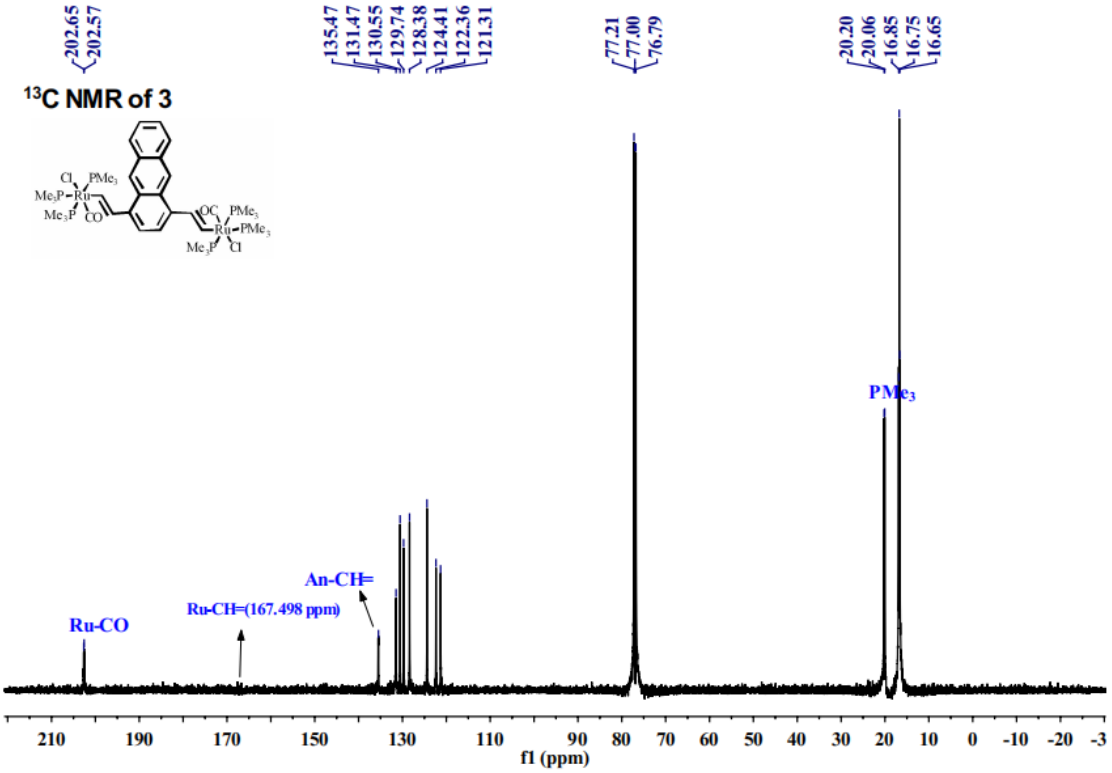

Figure S19. ^{13}C NMR spectrum (100 MHz, $CDCl_3$) of **3**.

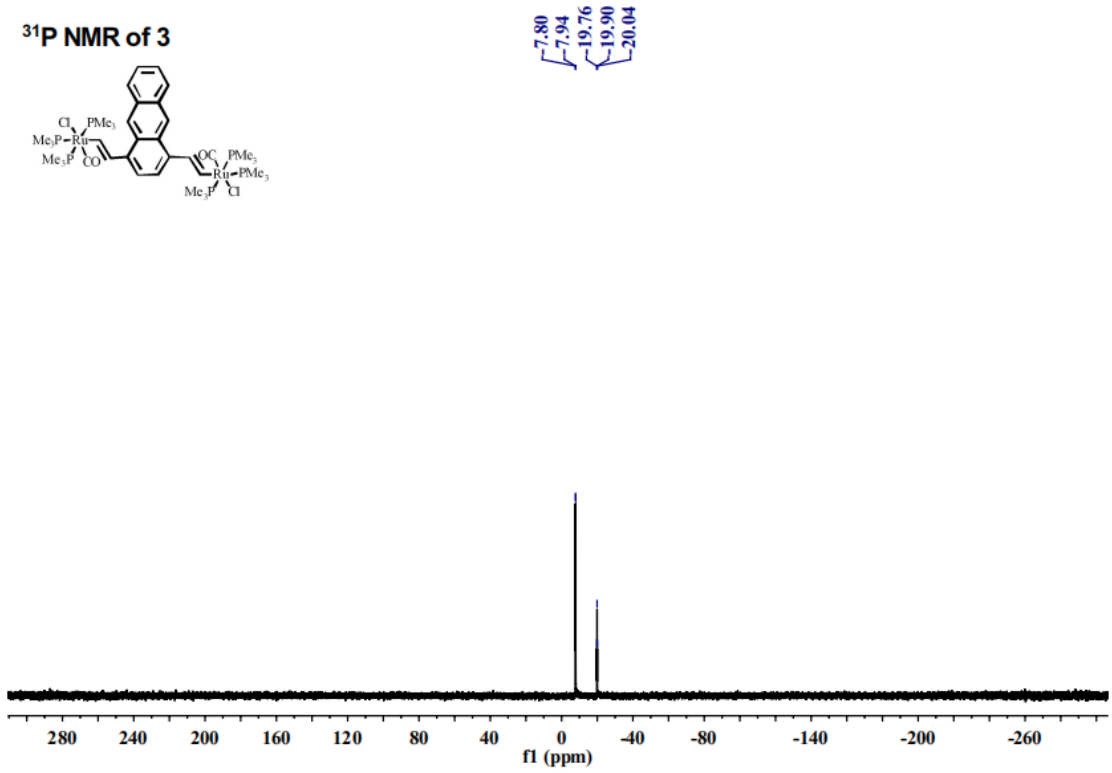

Figure S20. ^{31}P NMR spectrum (160 MHz, $CDCl_3$) of **3**.

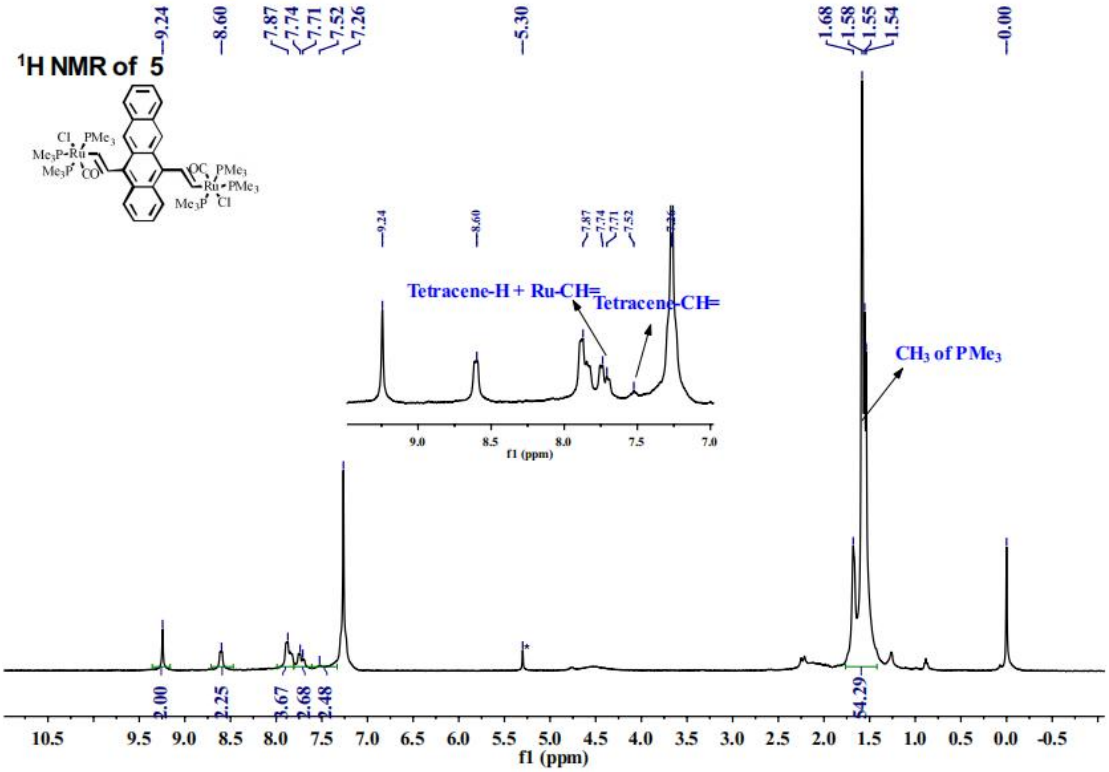

Figure S21. ^{1}H NMR spectrum (400 MHz, $CDCl_3$) of **5**.

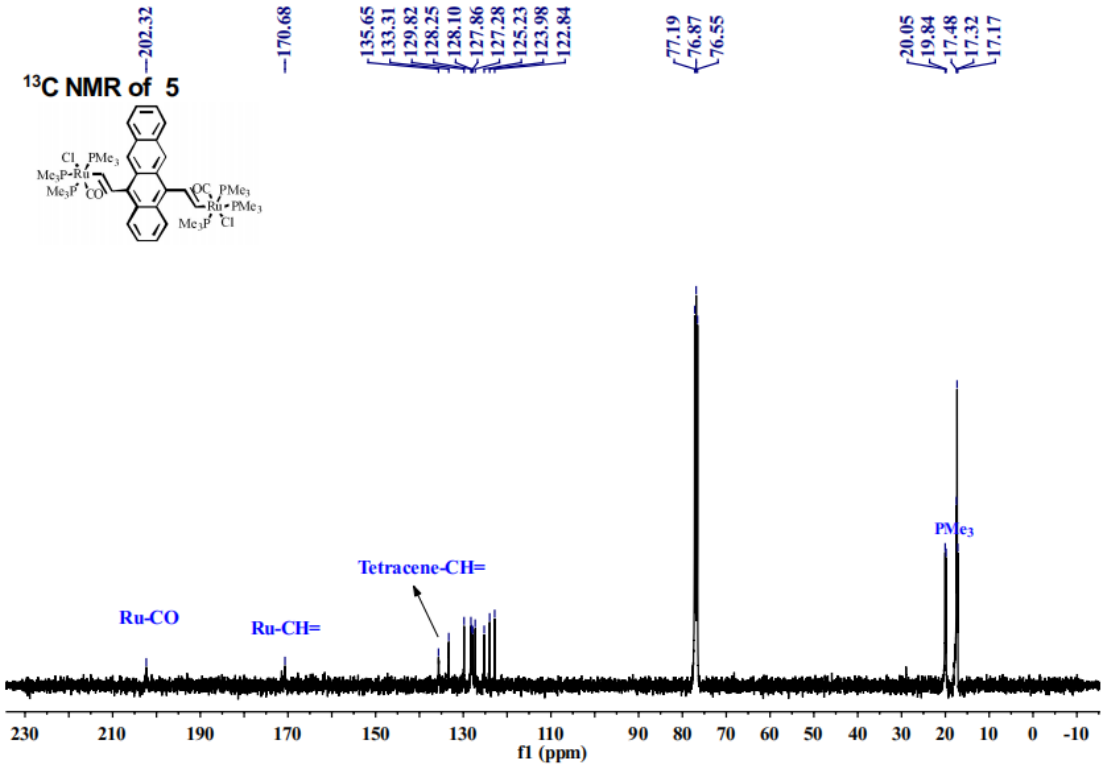

Figure S22. ^{13}C NMR spectrum (100 MHz, $CDCl_3$) of **5**.

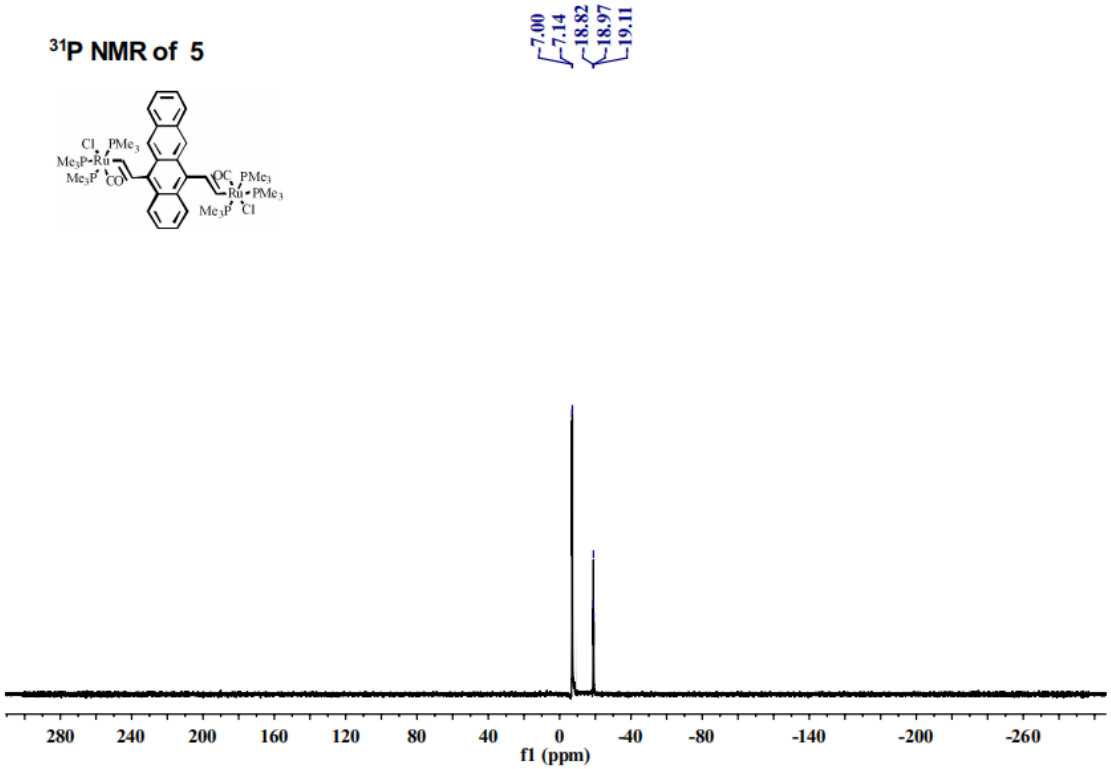

Figure S23. ^{31}P NMR spectrum (160 MHz, $CDCl_3$) of **5**.

7. Reference

1. N. Ahmad, J. J. Levison, S. D. Robinson, M. F. Uttley, E. R. Wonchoba, G. W. Parshall, *Inorg. Synth*. 1974, **15**, 45–64.
2. (a) S. E. Wheeler, A. J. McNeil, P. Müller, T. M. Swager, K. N. Houk, *J. Am. Chem. Soc*., 2010, **132**, 3304–3311; (b) J. H. Park, D. S. Chung, J. W. Park, T. Ahn, H. Kong, Y. K. Jung, J. Lee, M. H. Yi, C. E. Park, S. K. Kwon, H. K. Shim, *Org. Lett.*, 2007, **9**, 2573–2576.
3. Y. Hou, P. Wan, *Can. J. Chem.*, 2007, **85**, 1023–1032.
4. W. Y. Man, J-L. Xia, N. J. Brown, J. D. Farmer, D. S. Yufit, J. A. K. Howard, S. H. Liu, P. J. Low, *Organometallics* 2011, **30**, 1852–1858.
5. Y-P. Ou, J. Zhang, M. Xu, J. Xia, F. Hartl, J. Yin, G-A. Yu, S. H. Liu, *Chem. Asian J*. 2014, **9**, 1152–1160.
6. (a) M. Krejčík, M. Daněk, F. Hartl, *J. Electroanal. Chem. Interfacial Electrochem*., 1991, **317**, 179–187; (b) T. Mahabiersing, H. Luyten, R. C. Nieuwendam, F. Hartl, *Collect. Czech. Chem. Commun*., 2003, **68**, 1687–1709.
7. G. M. Sheldrick, SHELXS-97, a Program for Crystal Structure Solution; University of Göttingen: Göttingen, Germany, 1997.
8. G. M. Sheldrick, SHELXL-97, a Program for Crystal Structure Refifinement; University of Göttingen, Göttingen, Germany, 1997.
9. M. J. Frisch, G. W. Trucks, H. B. Schlegel, G. E. Scuseria, M. A. Robb, J. R. Cheeseman, G. Scalmani, V. Barone, B. Mennucci, G. A. Petersson, H. Nakatsuji,M. Caricato, X. Li, H. P. Hratchian, A. F. Izmaylov, J. Bloino, G.

Zheng, J. L. Sonnenberg, M. Hada, M. Ehara, K. Toyota, R. Fukuda, J. Hasegawa, M. Ishida, T. Nakajima, Y. Honda, O. Kitao, H. Nakai, T. Vreven, J. A. Montgomery, Jr., J. E. Peralta, F. Ogliaro, M. Bearpark, J. J. Heyd, E. Brothers, K. N. Kudin, V. N. Staroverov, R. Kobayashi, J. Normand, K. Raghavachari, A. Rendell, J. C. Burant, S. S. Iyengar, J. Tomasi, M. Cossi, N. Rega, J. M. Millam, M. Klene, J. E. Knox, J. B. Cross, V. Bakken, C. Adamo, J. Jaramillo, R. Gomperts, R. E. Stratmann, O. Yazyev, A. J. Austin, R. Cammi, C. Pomelli, J. W. Ochterski, R. L. Martin, K. Morokuma, V. G. Zakrzewski, G. A. Voth, P. Salvador, J. J. Dannenberg, S. Dapprich, A. D. Daniels, Ö. Farkas, J. B. Foresman, J. V. Ortiz, J. Cioslowski and D. J. Fox, Gaussian 09, Revision D.01, Gaussian, Inc., Wallingford CT, 2009.

10. M. Cossi, N. Rega, G. Scalmani, V. Barone, *J. Comput. Chem*. 2003, **24**, 669−681.
11. P. v. R. Schleyer, C. Maerker, A. Dransfeld, H. Jiao, N. J. R. van Eikema Hommes, *J. Am. Chem. Soc*. 1996, **118**, 6317−6318.